B. N. SEAL JOURNAL OF SCIENCE
ISSN: 0975-5624
PEER-REVIEWED JOURNAL
https://bnsealjournal.ac.in/

RESEARCH ARTICLE

Received: 11-03-2026
Accepted: 30-03-2026
Published: 09-04-2026

Citation: Sk J, Ghosh S, Chattoraj KK, Mondal D. Dynamics in Response to Blue Space Configuration Transformation of Bagri-tract in Lower Gangetic Flood Plain, Eastern India. B. N. Seal Journal of Science 2026, 14:29-42. https://doi.org/10.5281/zenodo.19475794

DOI: 10.5281/zenodo.19475794

***Corresponding Author:**
Email: *kuntalchattoraj@gmail.com*

Funding: None

Conflict of Interests: None

Published by:
Office of the Principal,
Acharya Brojendra Nath Seal College, Cooch Behar, West Bengal, India-736101

Land Surface Temperature Dynamics in Response to Blue Space Configuration Transformation of Bagri-tract in Lower Gangetic Flood Plain, Eastern India

Juel Sk[1], Sasanka Ghosh[1], Kuntal Kanti Chattoraj[1*], Debabrata Mondal[2]

[1] Department of Geography, Kazi Nazrul University, Asansol, West Bengal, India
[2] Department of Geography, S.C. Bose Centenary College, Lalbagh, Murshidabad, West Bengal, India

Abstract: Blue spaces such as wetlands, ponds and rivers contribute significantly to regulating the local thermal environment. This study analyses the dynamics of LST along with the transformation of blue spaces across the Bagri region from 2000 to 2020 with 5 years interval. To detect the change in water bodies, multi-temporal satellite data are used, and also to figure out which indices, such as MNDWI and NDMI, are suitable to detect blue space identification. The results demonstrate that the extent of wetlands has significantly decreased during the study period, from about 30% of wetlands in 2000 to about 12–13% in 2020 ($R^2 \approx 0.89$). In addition, the intensity of the thermal environment has increased, with the maximum LST increasing from about 61.3°C to about 70.4°C. Landscape fraction analysis shows that the values of patch and edge indices have continuously decreased, while the extent of the core area has increased, indicating an integrated change in landscape composition. The multiple linear regression models indicate that landscape composition has a crucial effect on LST. Overall, the results of this study indicate that there is a close relationship between the reduction of blue space and the increase in surface temperature. Therefore, wetland conservation and integrated management of blue space are particularly important for maintaining ecological balance and reducing thermal stress.

Keywords: Land Surface Temperature, Blue space configuration, Modified Normalized Difference Water Index, Landscape fragmentation, Bagri tract

Introduction

Urban areas contribute to more than 70% of all economic and human activity throughout the world [1]. In addition, the majority of the cities in the global south experienced significant climatic change in the 21st century due to an increase in the intensity of anthropogenic activities [2]. Population increases in developing countries triggered multiple environmental issues. India, a familiar subtropical monsoon-dominated country, and most of the cities experienced a seasonal variation of climatic variables [3, 4]. LULC is an important variable over the earth's surface because it is the key factor for the reflection of the overall condition of any area; it can be changed by either natural or artificial causes. Several land cover segments contribute to meeting the needs of human beings, but anthropogenic activity, especially the

abrupt increase in urbanization, is the supreme parameter that has changed the landscape scenario [5–7]. Urban agglomeration, industrialization [8–11], and development in the economic and transport sectors [12, 13] are the important driving factors for the change of blue space. Additionally, terrestrial to outer space radiation exchange is negatively affected by the release of possible pollutants from different sectors, notably the concentration of aerosol and gaseous pollutants. To understand the overall configuration of urban settings and thermal conditions, one needs to know the spatiotemporal change in the pattern of the urban blue space. In the present context, significant blue space alteration was observed due to the rapid enhancement of urban sprawl to create an inverse environmental impact [14, 15]. The change of LULC at the city scale is a consequence of the change in the flow of energy [16] and materials [17]. For the spatio-temporal variability of energy at the city scale, the thermodynamic properties are the fundamental indicators. The material used in the building helps to change energy fluctuation in the urban area because different ingredients of building materials have different heat-absorbing and -reflecting capacities [18, 19]. LST change is one of the greatest challenging issues overwhelming the world. LST is the interface temperature between the ground surface and atmosphere [20–23] and can assist in figuring out the water and energy dynamics at various geographic scales [24], including the city scale. The surface heat alteration at distinct places depends on the seasonal amount of solar beams [25, 26], but at the time of the dry winter season, boosting LST could be identified rather than in the hot humid season due to the increase in the sensible heat flux in winter [27, 28]. Also, LST is increased at night in urban areas more than during the day [27]. Concretization has made impervious surfaces instead of the natural segment, like blue and green space, leading to a dramatic change in LST [29]. The modification of the natural environment can cause a series of environmental issues as well as a profound impact on human life. Subsequently, an increase in temperature affects the thermal environment, which roadblocks sustainable urban development. The modernization of urbanism can influence energy consumption and, as a result, lead to the generation of artificial heat, increased gas emissions, and drastic changes in microclimate. Increase in temperature in urban areas in comparison to their surroundings due to anthropogenic causes known as "urban heat islands", which have multifaceted effects on the natural environment. The morphology of the city is a significant driver for change in LST [30]. Based on the literature reviews, the following research questions are framed: i) how do different spectral indices vary in their effectiveness result? ii) What are the temporal changes and trends observed about LST across the study area? iii) What is the scenario observed in landscape fragmentation in the selected study area? iv) What is the relationship between blue space, landscape fragmentation indices, and LST? Therefore, in this study, based on these research questions, two objectives are tried to find out i) to compare the effectiveness of different spectral indices, namely MNDWI, NDWI, NDMI, WRI, and MBSR, for accurate temporal analysis of blue space from 2000 to 2020. ii) To examine the relationship between blue space fragmentation, landscape indices, and LST.

Materials & Methods

Study area

The Bengal Basin's western part of the Bhagirathi River, known as the Rarh tract, and the eastern part, called the Bagri tract (Figure 1), reside at the confluence of the Bhagirathi, Padma, and Jalangi rivers, permeated by several offshoots of these rivers. This low-lying area, prone to annual inundation, often benefits from deposits of fertile silt, although occasional floods cause suffering.

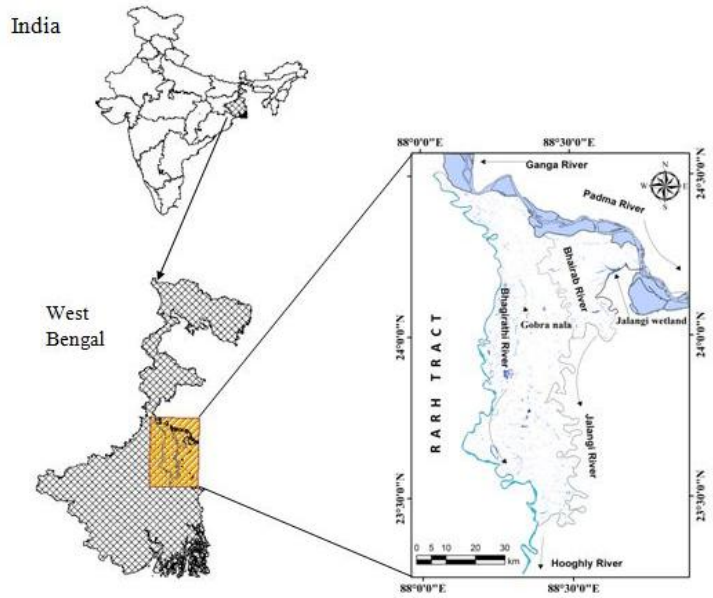

Figure 1: Location of the study area (Bagri tract).

The Bagri tract, located in the moribund delta of the Bengal Basin, features the Bhagirathi River, which represents the ancient channel of the Ganges, constrained by dense laterite soil that prevented westward flow and established the Bengal alluvium's limit. This region encompasses active channels, extensive floodplains, and diverse fluvial landforms, including river islands, oxbow lakes, and cut-off meanders, shaped by rivers such as the Padma and Bhagirathi. Approximately 22% of the area consists of unconsolidated materials like sand and silt. The major floodplains are formed by perennial rivers, while minor floodplains, adjacent to non-perennial channels, are less active. A robust river network, including the Jalangi, Bhairab, Pagla, Gorba nalla, and Suti nadi, sustains seasonally flooded wetlands. Seasonal floodplains like Pat Beel, Raman Beel, and Sialmari Beel, created by the combined effects of rivers such as the Bhagirathi, Jalangi, Brahmani, and Pagla, lie within this region, typically inundated annually. The area, with an average elevation of ~15 m above mean sea level, is characterized by thick alluvial soils of recent origin and a gentle topographic gradient of 0.19 m/km, constrained between the Bhagirathi River to the east and the para-deltaic fan surface to the west.

Data source

This study uses satellite imagery to derive various types of spatial maps. The required satellite data was collected from the official data portal of the United States Geological Survey (USGS), Earth Explorer. Satellite images with a spatial resolution of 30 meters were collected for the period 2000 to 2020. For the time-based change analysis, the data were selected at 5-year intervals, i.e., satellite images from 2000, 2005, 2010, 2015, and 2020 were used. The spectral bands used in the study are Blue, Green, Red, Near-Infrared (NIR), Mid-Infrared (MIR), and Short-Wave Infrared (SWIR). All these bands were collected from Landsat 7 and Landsat 8 OLI satellite imagery. There are four blue spaces that were selected based on the hydrological condition, especially focused on the seasonal water dynamics.

Methodology

The entire work was performed in Google Earth Engine, including the use of atmospherically corrected surface reflectance data, QA-based cloud and shadow masking, and the selection of images with less than 10% cloud cover. The key focus of this study is to assess the impact of wetlands on LST in the selected study area. So, for blue space, various methods are used, such as NDWI, MNDWI, WRI, NDMI, MBSR, and water transform. To search the relationship between landscape fragmentation and LST, a multiple linear regression model is used, with LST as the independent variable affected by the different landscape matrices that are Core, Edge, Patch and Perforated area.

Indices for Extraction of Blue Space

In this study, six different indices are used for the extraction of water bodies, as no single index is universally accepted. Here, NDWI and MNDWI are two indices used for this purpose, where the threshold value > 0 is considered as a water body. Though the threshold values vary depending on the environmental conditions, quality of sensor, etc., but in this study, initially, a threshold value > 0 is considered, further refined through satellite image visualization [31]. Also stated in their study that water bodies can be identified where NDWI values are greater than 0. The modified NDWI are used to get an improved version of accuracy based on the local conditions, where the threshold value is similar to that of NDWI. Further to validate the data, a total of 300 sample points was collected from Google Earth Pro and the kappa was used for validation. Here, the Kappa coefficient values for the years 2010, 2015 and 2020 are 0.79, 0.82, and 0.85, respectively.

Water Ratio Index (WRI)

Since the water reflectance value is higher in the green (Band 2) and red (Band 3) bands than in the near-infrared (Band 4) and mid-infrared (Band 5) bands, the Water Reflectance Index (WRI) generally exhibits a value greater than 1 for water bodies. Therefore, WRI is used as an effective index for water body identification, and its equation is as follows:

$$WRI = \frac{B_{Green} + B_{Red}}{B_{NIR} + B_{SWIR_1}} \quad \text{(Eq.1)}$$

Where, B = the reflectance values of the spectral bands, Band 3 = Green, Band 4 = Red, Band 5 = Near Infrared, NIR, and Band 6 = Shortwave Infrared 1, SWIR1 [32].

Normalized Difference Water Index (NDWI)

Since water reflectance is higher in the green and red bands, the Water Reflectance Index (WRI) usually shows a value greater than 1 for water bodies. Therefore, WRI is used to identify water bodies, and its equation is as follows:

$$NDWI = \frac{Green - NIR}{Green + NIR} \quad \text{(Eq.2)}$$

Modified Normalized Difference Water Index (MNDWI)

Due to the limitations of the NDWI method, especially its inability to extract water bodies from built-up areas. This index more clearly displays water characteristics and increases the accuracy of blue space identification by reducing the influence of built-up areas and vegetation.

$$MNDWI = \frac{\text{Green} - \text{MIR}}{Green + MIR} \quad \text{(Eq.3)}$$

Multi-band Spectral Relationship

According to the spectral properties of water, the reflectance gradually decreases from the green band to the SWIR band. Generally, the reflectance in the green and red bands is higher than in the NIR and SWIR bands, and it is on the basis of this property that it is possible to distinguish water bodies from other land covers.

$$\text{MBSR} = \text{Green} + \text{Red} > \text{NIR} + \text{MIR} \quad \text{(Eq.4)}$$

Normalized Difference Moisture Index (NDMI)

The Normalized Difference Moisture (Water) Index (NDMI or NDWI) is a satellite-based index that is calculated based on the reflectance values of the NIR and SWIR bands. Since the SWIR band is sensitive to changes in plant water content, it is possible to determine the water status of plants more accurately by combining NIR and SWIR.

$$\mathrm{NDMI} = \frac{\mathrm{NIR}-\mathrm{MIR}}{\mathrm{NIR}+\mathrm{MIR}} \quad \text{(Eq.5)}$$

Water

Water Transform Index is an index for waterbody identification. Actually, it's the Remodified NDWI, which helps in identifying water bodies in satellite imagery. It is calculated based on the reflectance values in the red and mid-infrared (MIR) bands. The equation is as follows:

$$WATER = \frac{\mathrm{Red}-\mathrm{MIR}}{Red+MIR} \quad \text{(Eq.6)}$$

Land Surface Temperature (LST)

Land Surface Temperature (LST) is the radiative skin temperature of the land surface, derived from thermal infrared sensor data (e.g., Landsat 8/9 Band 10) within the Google Earth Engine environment. The process involves converting raw digital numbers (DN) to radiance, then to Top-of-Atmosphere (TOA), Brightness Temperature (BT), and finally applying emissivity correction.

Top of the Atmosphere (TOA)

$$L\varphi = RM \times QCAL + RA \quad \text{(Eq.7)}$$

Where, $L\varphi$ indicates top of the atmosphere spectral radiance, measured in $WI(m^2.sr.\mu m)$, RM shows the radiance of Mult Band (from metadata file, MTL), QCAL represents Pixel values of the calibrated and quantized standard product (DN), and RA indicates radiance of Add Band (from metadata file, MTL).

Brightness Temperature ($\mathcal{J}$)

Spectral radiance is converted to brightness temperature ($\mathcal{J}$) using the thermal constants.

$$\mathcal{J} = \frac{K_2}{\ln(\frac{K_1}{L_\varphi}+1)} - 273.15 \quad \text{(Eq.8)}$$

Where $\mathcal{J}$ = At sensor brightness temperature (˚C), K1, K2 = Band-specific thermal conversion constants (from metadata), $L\varphi$ = TOA spectral radiance, 273.15 is subtracted to convert Kelvin to Celsius.

Normalized Difference Vegetation Index (NDVI)

NDVI is frequently utilized in remote sensing studies to represent vegetation cover and surface characteristics. It indicates the health and density of vegetation by measuring the difference between the NIR (which vegetation strongly

reflects) and the RED band (which vegetation absorbs). NDVI range varies from -1 to +1, higher NDVI values (+1) generally represent abundant and healthy vegetation, while lower values (-1) indicate barren land, built-up areas or water bodies.

$$\mathbf{NDVI} = \frac{(\mathbf{NIR}-\mathbf{Red})}{(\mathbf{NIR}+\mathbf{Red})} \quad \text{……..……..……(Eq.9)}$$

Proportion of Vegetation (Pv)

$$\mathbf{P_v} = \left(\frac{\mathbf{NDVI}-\mathbf{NDVI_{min}}}{\mathbf{NDVI_{max}}-\mathbf{NDVI_{min}}}\right) \quad \text{……..……(Eq.10)}$$

Where, $NDVI_{max}$ and $NDVI_{min}$ represents the maximum and minimum values of NDVI.

Emissivity (€)

Surface emissivity is commonly estimated using the NDVI threshold method.

$$\mathbf{\epsilon = 0.004 \times P_v + 0.986}$$

LST (Ƭ)

$$\mathbf{Ƭ} = \frac{\mathcal{J}}{\mathbf{1}+\left(\frac{\varphi \times \mathcal{J}vl}{P}\right)\ln(\epsilon)} \quad \text{…… (Eq.11)}$$

Where, Ƭ = Land surface temperature, $\mathcal{J}$ = Brightness of temperature, φ = Wavelength of emitted radiance, vl = Velocity of light, P = Boltzmann constant, € = Land surface emissivity, Ln = Log normal.

Multiple Linear Regression Model (Y)

This allows us to determine the relative impact of different independent variables on changes in the dependent variable. The equation is as follows:

$$\mathbf{Y} = \chi_0 + \chi_1 \epsilon_1 + \chi_2 \epsilon_2 + \chi_3 \epsilon_3 + \cdots + \chi_n \epsilon_n + \rho \text{……} \quad \text{(Eq.12)}$$

where, Y= dependent factor, χ = parameter, ϵ = independent factor, ρ = error

Results

To identify blue spaces, four representative blue spaces were selected and analyzed using six different indicators (Figure 2). The area of each blue space was then calculated to compare the performance of the different indicators.

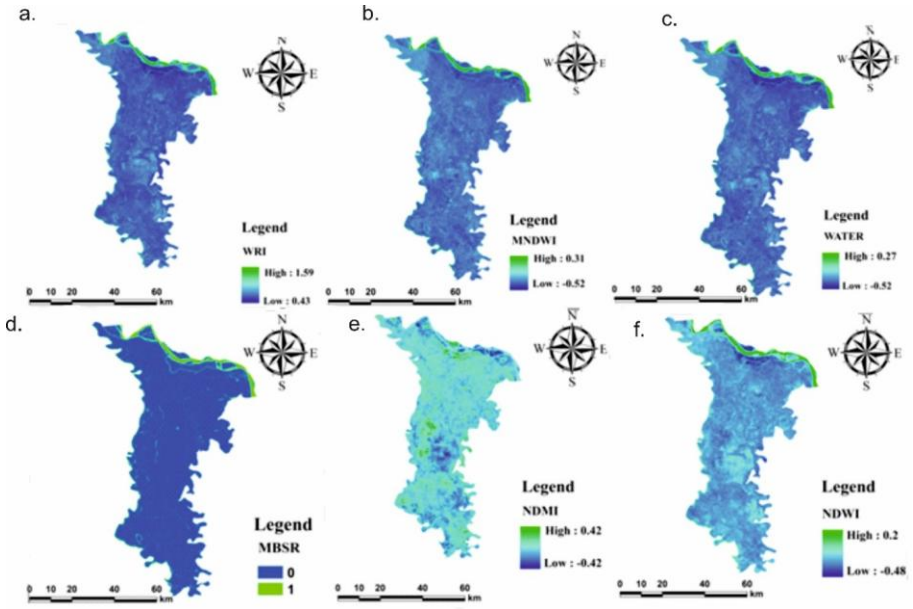

Figure 2: Spatial distribution of water extraction indices used in the study: (a) WRI, (b) MNDWI, (c) WATER, (d) MBSR, (e) NDMI, and (f) NDWI.

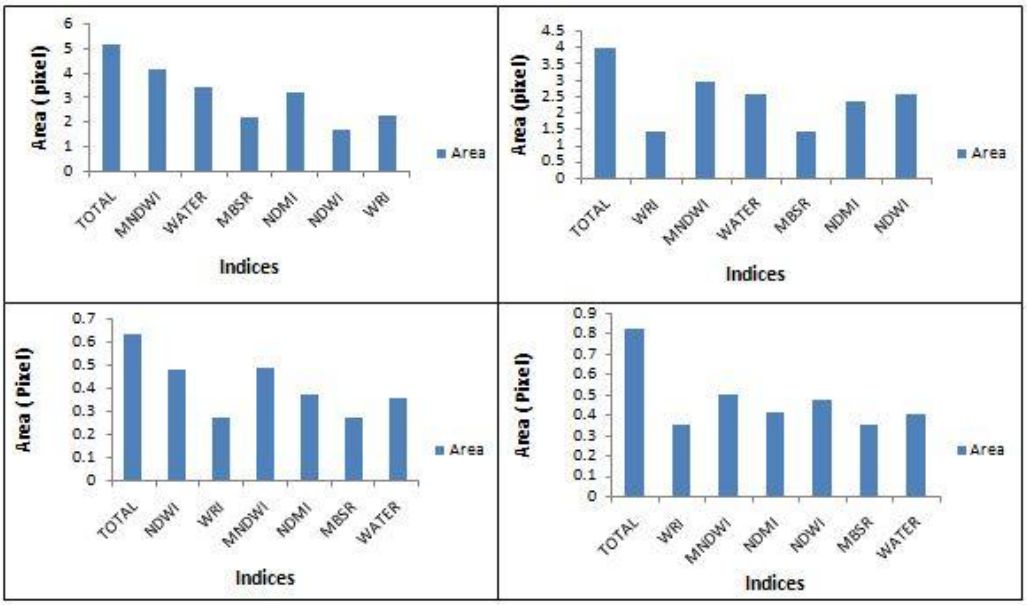

Figure 3: Area of blue space derived using different spectral indices.

The four bar charts in Figure 3 together demonstrate a continuous decrease in the total detected water area from the first panel to the last panel, indicating a decreasing trend of surface water expansion in the analyzed datasets. MNDWI

always detects relatively larger water areas than the other indices, which proves its high sensitivity in detecting water features in the region. NDWI and NDMI show moderate performance and often give values close to the WATER reference class, although the detected area is smaller than MNDWI. MBSR and WRI generally detect relatively smaller water areas, indicating low sensitivity. The relative order of the indices in all panels is generally the same, with MNDWI at the top, followed by NDWI and NDMI, and MBSR and WRI at the bottom. The slight fluctuation in area indicates differences in the thresholds and regional variability of the indices. The MNDWI may detect larger water bodies due to its reduced built-up and vegetation interference. NDWI may under-estimate the small or soil-mixed water fraction. NDMI contains moisture-related variability, which gives moderate performance. The spectral ratio dependence of MBSR makes it less sensitive. WRI detects relatively less, especially in isolated or shallow water areas. The decrease in total water area in increasing panels indicates a potential shrinkage of surface water. This trend may be due to seasonal changes, long-term climate change, or anthropogenic influences. The relative performance of the indices remains constant over a series of sequences. Minor discrepancies in detection indicate the influence of local land structure or atmospheric conditions. Overall, the results confirm the usefulness of MNDWI for accurate water point identification. NDWI and NDMI are useful for moderate detection. MBSR and WRI are less reliable but can provide information in specific contexts. Comparative analysis shows both changes in water extent and variability of indices over time. Understanding this pattern is important for blue space monitoring and management. The importance of index selection is clear, as it helps to capture accurate spatial blue space patterns. Monitoring temporal changes requires the use of sensitive and consistent indices. Ultimately, MNDWI emerges as the most effective indicator for water detection in the current study, and the reduction in area implies temporal changes in water expansion.

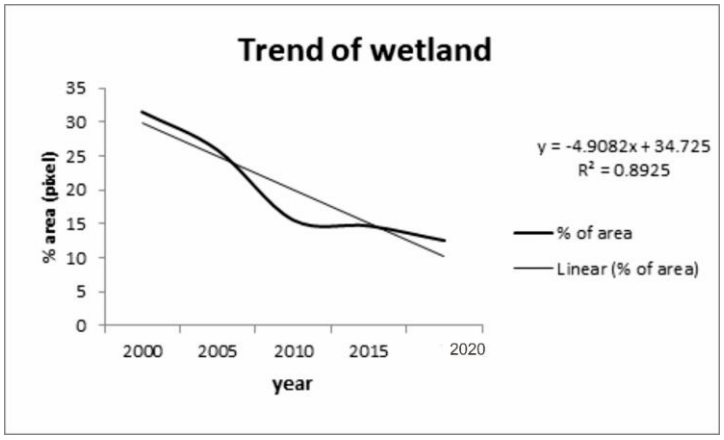

Figure 4: Temporal trend of blue space reduction during the period 2000–2020.

Figure 4 shows a clear and consistent trend of blue space loss between 2000 and 2020. The black line shows that the percentage of observed wetlands has been decreasing over time. In 2000, wetlands were around 30%, which decreased to around 15–20% around 2010, and stabilized at around 12–13% between 2015 and 2019. This consistent decrease clearly indicates that wetlands are shrinking rapidly. The gray line shows the overall trend of decline. Its slope is −4.9082, which indicates a decline of around 4.9% per unit of time. The R^2 value of 0.8925 indicates that there is a strong negative relationship between time and wetland area. Wetland loss has profound negative impacts on natural reservoirs, ecosystems, and biodiversity (Figure 5). It is also detrimental to water purification, wildlife habitat, and climate regulation. Some of the fluctuations in the figure also indicate the effects of local or seasonal changes. In the long term, this shrinkage may also affect human settlements, agriculture and urban management. Wetland depletion not only reduces water resources but also has the potential to disrupt the ecological balance. Therefore, effective monitoring, conservation and restoration measures are of utmost importance. Overall, this rapid and continuous wetland shrinkage is an important warning sign for us, emphasizing the importance of monitoring and conservation.

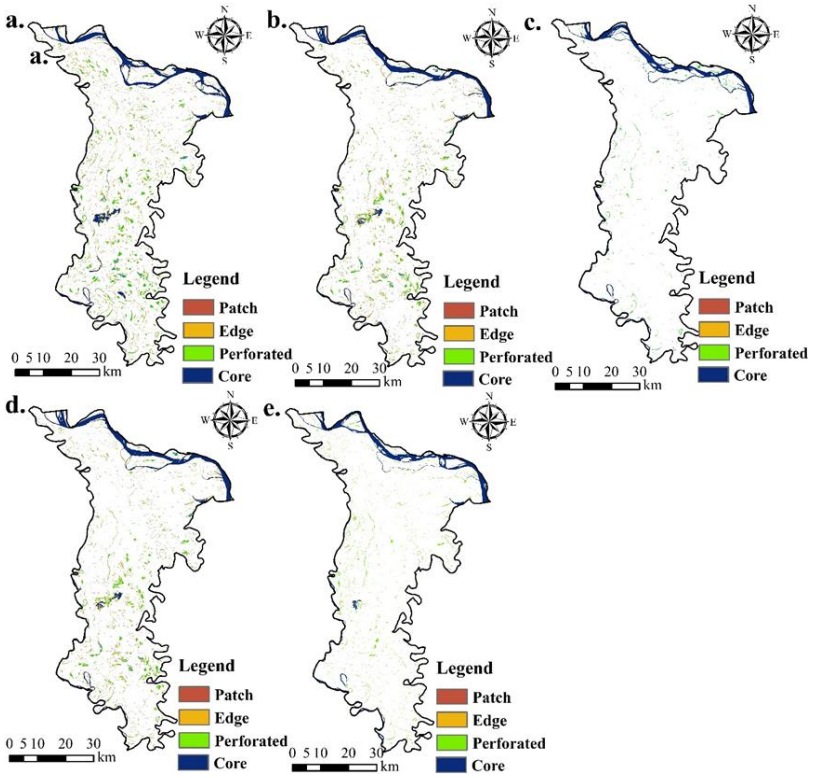

Figure 5: Fragmentation pattern of blue spaces in the Bagri tract from 2000 to 2020 at five-year intervals.

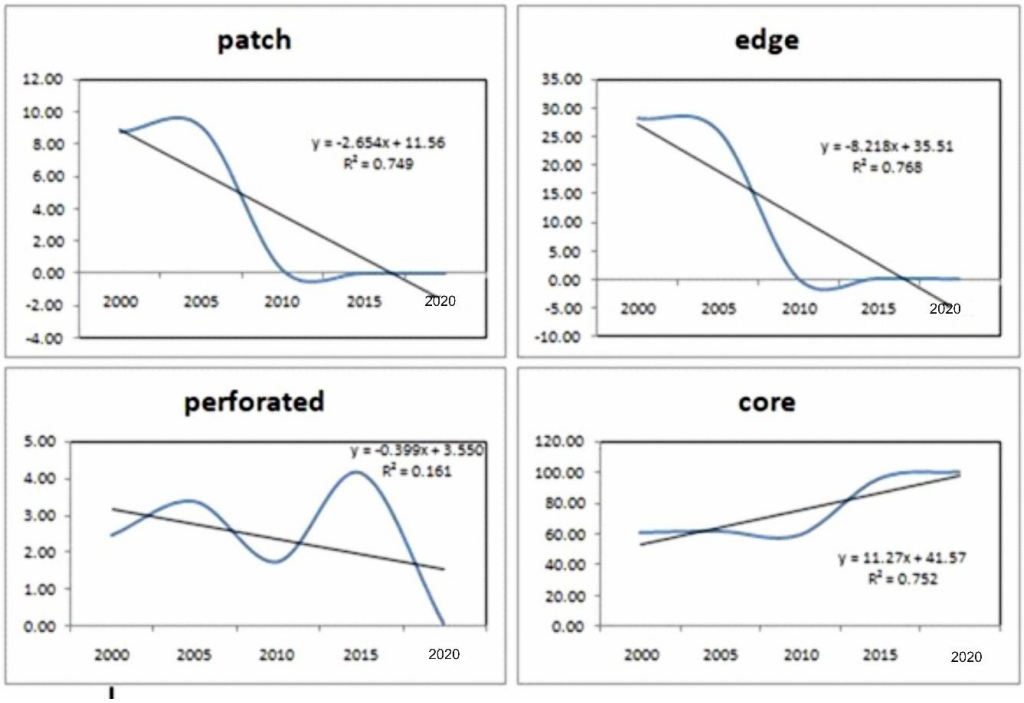

Figure 6: Temporal trends of landscape fragmentation metrics (patch, edge, perforated, and core) from 2000 to 2020 at five-year intervals.

Figure 6 illustrates changes in four landscape fragmentation metrics – patch, edge, perforated, and core – between 2000 and 2020. The Patch value gradually decreased from 8.7 to almost zero in 2020 (slope −2.654x, $R^2 = 0.749$), indicating the rapid disappearance or disappearance of small landscape areas. The Edge value also decreased from about 28 to 0 (slope −8.218x, $R^2 = 0.768$), indicating the reduction in complexity of fragment boundaries and changes in local microclimate. The Perforated value fluctuated, increasing to about 4.0 in 2015 but decreasing in 2020 (slope −0.399x, $R^2 = 0.161$), reflecting the temporary increase in small gaps or cavities. In contrast, the core area has gradually increased from around 60 in 2000 to around 100 in 2020 (slope 11.27x, $R^2 = 0.752$), indicating the preservation and expansion of the central stable part.

The rapid decline of patch and edge, the fluctuation of perforated, and the continuous increase of core indicate that both fragmentation and central stability of the landscape are important. These changes are relevant for local environmental impacts such as temperature regulation, reservoir efficiency, and biodiversity. By monitoring fragment shrinkage and core expansion, it is possible to take effective measures in urban planning and nature conservation. In the long term, this trend is important for urban ecosystem management and climate stability. In addition, this information can be used in local ecosystem and forest planning to improve urban temperature regulation and water management. These changes in the landscape over time show that maintaining ecological balance and coordinating urban planning are essential.

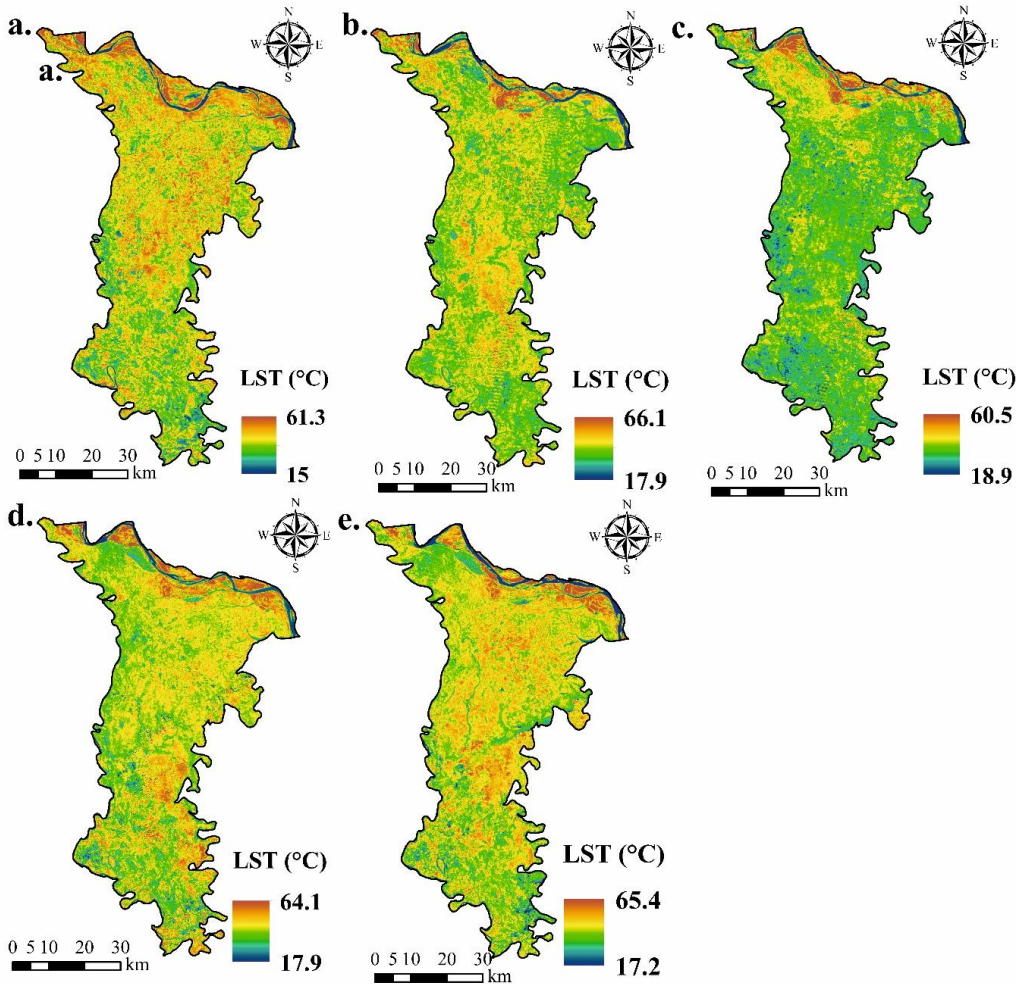

Figure 7: Spatio-temporal variation of LST in the study area from 2000 to 2020 at five-year intervals.

Figure 7 reflects the spatio-temporal alterations in LST at five-year intervals from 2000 to 2020. A comparative analysis of the maps demonstrates that the high-temperature zone has undergone an increase over time, and the density of thermal hotspots has also become more pronounced. The 2000 map (a) shows the range of land surface temperatures (LST) from about 15°C to 61.3°C. During that time, most regions experienced above-average temperatures, as reflected in green and yellow. The relatively high temperature areas are located in different locations, mainly in the north and northeast. The 2005 map (b) shows the temperature range increasing from about 17.9°C to 66.1°C, and the expansion of the hot zone becomes more pronounced, especially in the central and northern parts. The 2010 map (c) shows the maximum temperature decreasing slightly to about 60.5°C, while the minimum temperature is about 18.9°C. However, the relatively cold areas in the south are more pronounced. It is likely that these areas have dense vegetation or wetlands, which help to reduce the temperature. The 2015 map (d) shows the temperature trend again, and the maximum LST reaches about 64.1°C, while the minimum temperature is about 17.9°C. During this time, the hot zones appear to be more widespread and denser, especially in the northern and central regions. Finally, the 2020 map (e) shows the maximum temperature increasing to about 65.4°C, while the minimum temperature is about 17.2°C. During this time, the areas of high temperatures shown in orange and red have expanded greatly, and the density of thermal hotspots has increased, especially in the north and central regions. In comparison, the relatively cold areas are mainly confined to the south.

Overall, an analysis of the above series of maps shows that an increasing trend of land surface temperature has been observed in the study area during the period from 2000 to 2020, and the spatial extent of the high temperature region has gradually expanded. As a result, it is assumed that a significant change has occurred in the thermal environment of the region during that period.

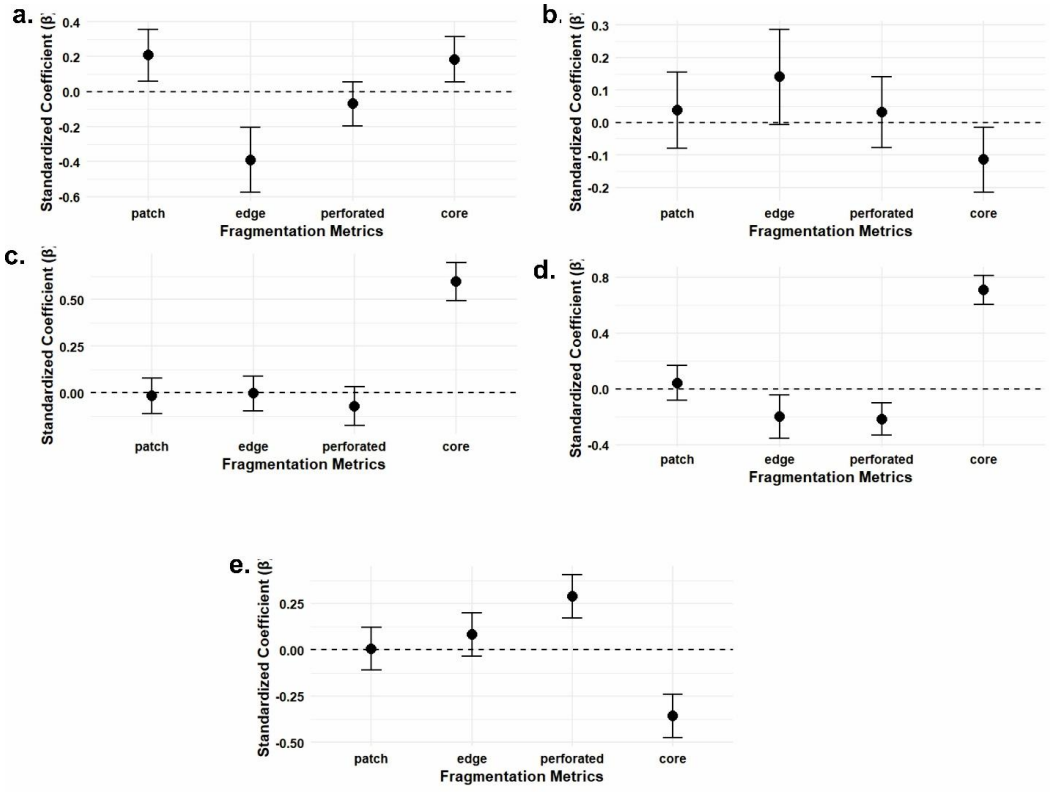

Figure 8: Standardized coefficients (β) of fragmentation metrics on LST (a–e).

Multiple linear regressions are mainly used to see the relationship between the dependent variable and more than one independent variable. Here, this model is used to determine the relationship between landscape fragmentation metrics that are patch, edge, perforated, core and LST. VIF values of 1.00-1.32 refer to multicollinearity test results within the acceptable range, and variables are distinct from one another. Figure 8 revealed that in the years 2000 and 2005, the landscape metrics could explain LST only to a limited extent, with the Adjusted R^2 values of 0.032 and 0.229, respectively. But in 2010, the explanatory power increased to 0.177. But it got picked in the year 2015. It decreased again in 2020, indicating that the influence of other uncontrolled factors may increase in the future. The core area consistently emerged as the most important variable. In 2010 and 2015, it was observed that the p-value is <0.001, which is less than the threshold level, indicating that large and connected core areas are closely related to temperature changes. In 2020, a similar result was observed. Edge metric shows a clear relationship with LST in 2000 and 2015, i.e. edge characteristics can affect temperature in certain situations. Perforated metric has a limited but statistically significant effect on LST in specific years. In some years, it is observed that the patch area does not achieve a significant level ($p < 0.05$), which reveals that patch size alone does not play as a driving factor for LST. The core area consistently emerged as the most important variable. In 2010 and 2015, it was observed that the p-value is <0.001, which is less than the threshold level, and the β values are 0.597 and 0.710, respectively, indicating that large and connected core areas are positively related to temperature changes. In 2020, a similar result was observed, where the β value is 0.653. On the other hand, edge density is negatively related to LST in 2000 ($\beta = -0.390$, $p < 0.001$) and 2015 ($\beta = -0.200$, $p = 0.012$). Similarly, perforation shows mixed effects, with a negative relationship in 2015 ($\beta = -0.216$, $p < 0.001$) and a positive one in 2020 ($\beta = 0.291$, $p < 0.001$). Therefore, this ensures that a relationship exists between landscape matrices and LST, but it varies over time. Along with landscape matrices, LST also depends on the structure and connectivity of the landscape. In urban planning, expanding green space is not sufficient. So, equal attention must be given to preserving the spatial structure and ensuring proper connectivity within the landscape.

Discussion

The analysis of different blue space indices shows that there is a significant difference in the performance of different spectral indices used to determine blue space. Among the indices tested, MNDWI has always been able to identify a relatively higher blue space. The main reason for this is the combined use of green and SWIR bands, which greatly reduces the influence of built-up land and vegetation and helps to determine the actual wetland more clearly. Many of these studies prove that MNDWI is a suitable method for the extraction of water bodies [33, 34].on the other hand, NDWI and NDMI have given mediocre results, which in many cases have shown relatively lower values than the actual blue space. The WRI and MBSR indices have relatively low blue space, which indicates the limitations of their sensitivity. Therefore, it is important to choose the appropriate index for blue space identification. Time-based analysis shows that blue space has gradually decreased in the study area from 2000 to 2020, which reveals the gradual shrinkage of blue space. Landscape matrix analysis shows that there have been significant changes in the indices related to fragmentation. The values of patch and edge indices have decreased, but the core part has gradually increased. The decrease in patch and edge indicates the disappearance of small and isolated landscapes and the reduction of boundary complexity. On the other hand, the expansion of the core area reveals the development of a large and stable landscape. These changes may have important effects on temperature regulation [35].

LST analysis shows that temperatures have gradually increased from 2000 to 2020. The spread of warm zones has increased, and the density of temperature ‘hotspots’ has increased. The relatively cold regions are mainly adjacent to green and wetlands. This indicates the important role of blue and green infrastructure in regulating local temperature. Multi-linear regression analysis shows a dynamic relationship between landscape indices and temperature. The core area index often appears to be the most influential. A strong positive relationship was observed between 2010 and 2015, indicating that large land blocks contribute to higher temperatures. In 2020, this relationship turned negative, indicating that the impact of temperature may also change with land cover and pattern changes. The effects of edge and perforation indices are relatively unstable and time-dependent.

Overall, the study demonstrates that there is a close relationship between blue space, land fraction, and temperature. The reduction of blue space and the change in landscape pattern have important impacts on the thermal environment of the region. Therefore, the conservation of blue space and appropriate land planning are essential for temperature regulation.

Conclusion

This study analyzed the relationship between blue space fragmentation and LST using various spectral indices. The results showed that MNDWI was the most effective in identifying blue space, while NDWI and NDMI showed moderate effectiveness. The amount of blue space gradually decreased from 2000 to 2020, indicating the shrinkage of blue space and may have a negative impact on the local temperature environment. The landscape fragmentation analysis revealed that the core area expanded, the number of small patches decreased, and the complexity of the boundaries decreased, indicating important changes in the landscape structure. Furthermore, the high-temperature zones increased. Multi-linear regression analysis showed that the landscape fragmentation matrix, especially the core area expansion, had a significant impact on the change in land surface temperature. These results indicate that maintaining ecological stability and regulating regional temperatures through wetland management, balanced landscape design, and blue space conservation are crucial.

Reference

1. Liu X, Zhou Y, Yue W, Li X, Liu Y, Lu D. Spatiotemporal patterns of summer urban heat island in Beijing, China using an improved land surface temperature. *Journal of Cleaner Production* 2020, 257:120529.
2. Anguelovski I, Chu E, Carmin J. Variations in approaches to urban climate adaptation: Experiences and experimentation from the global South. *Global Environmental Change* 2014, 27:156–167.
3. Siddiqui A, Kushwaha G, Nikam B, Srivastav SK, Shelar A, Kumar P. Analysing the day/night seasonal and annual changes and trends in land surface temperature and surface urban heat island intensity for Indian cities. *Sustainable Cities and Society* 2021, 75:103374.
4. Chalakkal JB, Mohan M. Is the Monsoon climatology observed over the National Capital Region, Delhi indicative of an Urban–Monsoon linkage on rainfall modification? *Urban Climate* 2022, 46:101289.
5. Kumar BP, Anusha BN, Babu KR, Sree PP. Identification of climate change impact and thermal comfort zones in semi-arid regions of AP, India using LST and NDBI techniques. *Journal of Cleaner Production* 2023, 407:137175.
6. Han J, Meng X, Zhou X, Yi B, Liu M, Xiang WN. A long-term analysis of urbanization process, landscape change, and carbon sources and sinks: A case study in China's Yangtze River Delta region. *Journal of Cleaner Production* 2017, 141:1040–1050.
7. Arghavani S, Malakooti H, Bidokhti AAA. Numerical assessment of the urban green space scenarios on urban heat island and thermal comfort level in Tehran Metropolis. *Journal of Cleaner Production* 2020, 261:121183.
8. Imdad K, Sahana M, Revetz J, Areendran G, Gautam O, Dwivedi S, Sajjad H. A sustainable solution to manage ecosystem health of wetlands in urban and peri-urban areas of Lucknow district, India using geospatial techniques and community based pragmatic approach. *Journal of Cleaner Production* 2023, 137646.
9. Saha S, Bera B, Shit PK, Bhattacharjee S, Sengupta N. Estimation of carbon budget through carbon emission-sequestration and valuation of ecosystem services in the extended part of Chota Nagpur Plateau (India). *Journal of Cleaner Production* 2022, 380:135054.
10. Tran DX, Pla F, Latorre-Carmona P, Myint SW, Caetano M, Kieu HV. Characterizing the relationship between land use land cover change and land surface temperature. *ISPRS Journal of Photogrammetry and Remote Sensing* 2017, 124:119–132.
11. Seyam MMH, Haque MR, Rahman MM. Identifying the land use land cover changes using remote sensing and GIS approach: A case study at Bhaluka in Mymensingh, Bangladesh. *Case Studies in Chemical and Environmental Engineering* 2023, 7:100293.
12. Cong C, Kwak Y, Deal B. Incorporating active transportation modes in large scale urban modeling to inform sustainable urban development. *Computers, Environment and Urban Systems* 2022, 91:101726.
13. Gounaridis D, Chorianopoulos I, Symeonakis E, Koukoulas S. A Random Forest-Cellular Automata modelling approach to explore future land use/cover change in Attica (Greece), under different socio-economic realities and scales. *Science of the Total Environment* 2019, 646:320–335.

14. Hamoodi MN, Corner R, Dewan A. Thermophysical behaviour of LULC surfaces and their effect on the urban thermal environment. *Journal of Spatial Science* 2019, 64(1):111–130.
15. Bokhari SA, Saqib Z, Amir S, Naseer S, Shafiq M, Ali A, Hamam H. Assessing land cover transformation for urban environmental sustainability through satellite sensing. *Sustainability* 2022, 14(5):2810.
16. Parbaleh A, Kaboli HS. Detection of trend changes in surface energy budget caused by urbanization and land cover/use changes in Dezful plain, Iran. *Environmental Earth Sciences* 2023, 82(11):283.
17. Pal S, Das P, Mandal I, Sarda R, Mahato S, Nguyen KA, Saha TK. Effects of lockdown due to COVID-19 outbreak on air quality and anthropogenic heat in an industrial belt of India. *Journal of Cleaner Production* 2021, 297:126674.
18. Zhang M, Zhang F, Chen D, Tan ML, Chan NW. Urban local surface temperature prediction using the urban gray-green space landscape and vegetation indices. *Building and Environment* 2022, 226:109723.
19. Akbari H, Kolokotsa D. Three decades of urban heat islands and mitigation technologies research. *Energy and Buildings* 2016, 133:834–842.
20. Duan SB, Li ZL, Li H, Göttsche FM, Wu H, Zhao W, Coll C. Validation of Collection 6 MODIS land surface temperature product using in situ measurements. *Remote Sensing of Environment* 2019, 225:16–29.
21. Sekertekin A, Bonafoni S. Land surface temperature retrieval from Landsat 5, 7, and 8 over rural areas: Assessment of different retrieval algorithms and emissivity models and toolbox implementation. *Remote Sensing* 2020, 12(2):294.
22. Thakur S, Maity D, Mondal I, Basumatary G, Ghosh PB, Das P, De TK. Assessment of changes in land use, land cover, and land surface temperature in the mangrove forest of Sundarbans, northeast coast of India. *Environment, Development and Sustainability* 2021, 23:1917–1943.
23. Tan J, Yu D, Li Q, Tan X, Zhou W. Spatial relationship between land-use/land-cover change and land surface temperature in the Dongting Lake area, China. *Scientific Reports* 2020, 10(1):9245.
24. Hu Y, Tang R, Jiang X, Li ZL, Jiang Y, Liu M, Zhou X. A physical method for downscaling land surface temperatures using surface energy balance theory. *Remote Sensing of Environment* 2023, 286:113421.
25. Jamil B, Siddiqui AT, Akhtar N. Estimation of solar radiation and optimum tilt angles for south-facing surfaces in humid subtropical climatic region of India. *Engineering Science and Technology, an International Journal* 2016, 19(4):1826–1835.
26. Chatzipoulka C, Compagnon R, Nikolopoulou M. Urban geometry and solar availability on façades and ground of real urban forms: using London as a case study. *Solar Energy* 2016, 138:53–66.
27. Peng J, Jia J, Liu Y, Li H, Wu J. Seasonal contrast of the dominant factors for spatial distribution of land surface temperature in urban areas. *Remote Sensing of Environment* 2018, 215:255–267.
28. Mohammad P, Goswami A. Predicting the impacts of urban development on seasonal urban thermal environment in Guwahati city, northeast India. *Building and Environment* 2022, 226:109724.
29. Portela CI, Massi KG, Rodrigues T, Alcântara E. Impact of urban and industrial features on land surface temperature: Evidences from satellite thermal indices. *Sustainable Cities and Society* 2020, 56:102100.
30. Zhou B, Rybski D, Kropp JP. The role of city size and urban form in the surface urban heat island. *Scientific Reports* 2017, 7(1):4791.
31. Ji L, Zhang L, Wylie B. Analysis of dynamic thresholds for the normalized difference water index. *Photogrammetric Engineering & Remote Sensing* 2009, 75(11):1307–1317.
32. Kareem H, Attaee M, Omran A. Estimation the water ratio index (WRI) and automated water extraction index (AWEI) of Bath in the United Kingdom using remote sensing technology of the multispectral data of Landsat 8 OLI. *Water Conservation and Management* 2024, 8:125–132.
33. Yue H, Li Y, Qian J, Liu Y. A new accuracy evaluation method for water body extraction. *International Journal of Remote Sensing* 2020, 41(19):7311–7342.
34. Sun Q, Li J. A method for extracting small water bodies based on DEM and remote sensing images. *Scientific Reports* 2024, 14(1):760.
35. Saha A, Saha S, Das A, Mandal S, Sarkar R, Das M. Unveiling the landscape fragmentation and its impact on land surface temperature using machine learning approach in Kolkata Metropolitan Area (India). *Theoretical and Applied Climatology* 2025, 156(7):384.